Smart Structures and Systems, *Vol. 32, No. 4 (2023) 235-251*
https://doi.org/10.12989/sss.2023.32.4.235

Extended artificial neural network for estimating the global response of a cable-stayed bridge based on limited multi-response data

Namju Byun [1a], Jeonghwa Lee [1b], Keesei Lee [2c] and Young-Jong Kang*[3]

[1] *Future and Fusion Laboratory of Architectural, Civil and Environmental Engineering, Korea University, Seoul 02841, Korea*
[2] *Department of Urban Infrastructure Research, Seoul Institute of Technology, Seoul 03909, Korea*
[3] *School of Civil, Environmental and Architectural Engineering, Korea University, Seoul 02841, Korea*

(*Received April 28, 2023, Revised September 1, 2023, Accepted October 10, 2023*)

Abstract. A method that can estimate global deformation and internal forces using a limited amount of displacement data and based on the shape superposition technique and a neural network has been recently developed. However, it is difficult to directly measure sufficient displacement data owing to the limitations of conventional displacement meters and the high cost of global navigation satellite systems (GNSS). Therefore, in this study, the previously developed estimation method was extended by combining displacement, slope, and strain to improve the estimation accuracy while reducing the need for high-cost GNSS. To validate the proposed model, the global deformation and internal forces of a cable-stayed bridge were estimated using limited multi-response data. The effect of multi-response data was analyzed, and the estimation performance of the extended method was verified by comparing its results with those of previous methods using a numerical model. The comparison results reveal that the extended method has better performance when estimating global responses than previous methods.

Keywords: multi-response data; neural network; response estimation; SHM; structural response

1. Introduction

Structural health monitoring (SHM) systems have been implemented and operated worldwide owing to the aging of structures, allowing the accumulation of a vast amount of measurement data (Koo *et al*. 2013, Sun *et al*. 2009, Wong 2004). In addition, techniques for utilizing the measurement data have been studied to monitor the health of the structure. Among these techniques, a method for estimating the unmeasured response has been investigated to evaluate the structural integrity through measurement data. Owing to the limitations of conventional displacement sensors, such as linear variable differential transformers and laser Doppler vibrometers, early research on unmeasured response estimation focused on estimating the displacement using acceleration, slope, and strain.

Acceleration meters have been widely adopted for dynamic displacement estimation because they are generally cost-effective, easy to install, and have low noise. Using acceleration, the displacement can be simply estimated by double integration, considering the initial velocity and displacement. However, significant bias error can occur if the initial conditions are not accurately considered. To eliminate the bias error, Park *et al*. (2005) proposed a method to estimate the initial velocity by assuming that the initial displacement and averaging differentiation of the estimated displacement are zero. Lee *et al*. (2010) developed a finite impulse response (FIR) filter that can reconstruct displacement in the time domain using measured acceleration without initial conditions. In the FIR filter, the displacement is reconstructed by minimizing the squared errors between the measured and approximated accelerations within a finite-time interval. In addition, an overlapping time window was introduced to improve accuracy. Subsequently, a wireless system for estimating displacement based on the FIR filter and using acceleration responses was developed and verified through laboratory tests (Park *et al*. 2013).

A disadvantage of the methods that use measured acceleration is that they can estimate displacement only at the measurement points because spatial parameters are not included in the acceleration response. In contrast, the slope and strain responses, including spatial parameters, can be used to estimate the displacement at any point of the structure. The shape superposition method (SSM) is the most widely used technique for estimating displacement using slope and strain. In a linear system, the global response of the structure can be represented as a superposition of shape functions weighted by their respective shape factors. The SSM can be applied to either displacement, slope, or strain. The optimal shape factor is generally calculated using the least squares method, which minimizes the square error between the measured response and the superposed shape functions weighted by the shape factors.

Hou *et al*. (2005) developed a bridge deflection measurement method based on the SSM using slope data. A

*Corresponding author, Ph.D., Professor,
E-mail: yjkang@korea.ac.kr
[a] Ph.D., E-mail: skawn0702@naver.com
[b] Ph.D., E-mail: qevno@korea.ac.kr
[c] Ph.D., E-mail: kslee@sit.re.kr

ISSN: 1738-1584 (Print), 1738-1991 (Online)

power series was adopted as the shape function, ensuring that the deflection curve satisfied the boundary conditions at the piers. The method was verified through laboratory and field experiments. Although estimation results using slope showed good performance, strain has been used for displacement estimation more frequently than slope owing to the low cost and convenient installation of the required sensors. Foss and Haugse (1995) first attempted to estimate displacement based on strain data by introducing a modal mapping method, which is similar to SSM in that it also uses a mode shape as the shape function. The shape factor was calculated using the least-squares method. Subsequently, Shin *et al*. (2012) developed a displacement estimation algorithm using fiber Bragg grating (FBG) sensors based on modal mapping. The sine function and theoretical mode shape were adopted as the shape functions and the algorithm was applied in field tests on various types of bridges. The mode shape derived from the frequency analysis of finite element models (FEM) was also applied to estimate displacement (Cho *et al*. 2015). The results showed that FEM mode shapes can estimate the displacement more accurately than the theoretical mode shape because structural characteristics are included in the FEM mode shape. Modal mapping has been used in many studies as a basic method to estimate displacement using strain (Deng *et al*. 2019, Kliewer and Glisic 2019, Li *et al*. 2017, Rapp *et al*. 2009). In addition, studies on data fusion of strain and acceleration data have been conducted based on modal mapping and Kalman filters to improve the accuracy of displacement estimation (Cho *et al*. 2014, Sarwar and Park 2020, Zhang *et al*. 2022). However, data fusion including acceleration data limits the range of displacement estimation to the location where the accelerometer is installed owing to the characteristics of acceleration, as mentioned before.

As global navigation satellite systems (GNSS) have been developed and improved, “structural response analysis using a limited amount of displacement data” (SRALD) has been proposed and verified with the FEM model of a cable-stayed bridge (Choi *et al*. 2017a). SRALD can estimate the global displacement and internal forces based on the SSM and least-squares method using the structural shape function derived through static numerical analysis. SRALD has been further extended to “structural response analysis using a limited amount of multi-response data” (SRALMR), which can estimate global displacement and internal forces by combining displacement, slope, and strain data to improve accuracy (Byun *et al*. 2022). Although various estimation methods based on SSM have been developed and applied as mentioned above, the least-squares method generally adopted in previous studies to calculate the optimal shape factor has a limitation as it minimizes the error between the estimated and measured responses only at the measurement point. This characteristic may lead to considerable estimation errors at locations where sensors are not installed.

Recently, machine learning algorithm such as support vector regression (SVR), decision tree (DT), random forest (RF), and artificial neural network (ANN) have been used in SHM as an alternative method to estimate or predict responses. Castellon *et al*. (2021) estimated dynamic response of Hardanger Bridge based on the SVR using full-scale wind data. Lei *et al*. (2023) proposed extreme Gradient Boosting method based on DT to estimate displacement of the cable-stayed bridge using temperature, wind, and traffic data. Ye *et al*. (2023) employed RF to predict the acceleration of cable-stayed bridges with a focus on wind-induced responses. In addition, ANN has been widely adopted for SHM due to its ability to learn complex patterns and relationships within structural data, enabling more accurate and efficient estimation and prediction. The displacement has been estimated using an ANN based on strain data (Moon *et al*. 2019) and a convolutional neural network (CNN) based on acceleration data (Wu and Jahanshahi 2019). Long short term memory (LSTM) also has been widely adopted to estimate dynamic displacement using wind speed (Xue and Ou 2021) or strain data (Duan *et al*. 2022). In addition, the strain has been estimated using a CNN based on wind and displacement data (Oh *et al*. 2019), and a LSTM model based on acceleration data (Gulgec *et al*. 2020). However, the responses in previous studies can only be estimated at specific points, or response data from too many locations are required to estimate global responses. Therefore, Byun and Kang (2023) proposed an estimation method based on SSM and an ANN that can estimate global deformation and internal forces using only a limited amount of displacement data.

In this study, the estimation method by Byun and Kang (2023) was extended to incorporate slope and strain data, in addition to displacement, and improve estimation accuracy. The extended algorithm is based on SSM and uses an ANN instead of the least-squares method to calculate the optimal shape factor. The extended parts and scope of this study are described below:

- The limited slope and strain data were additionally used as input variables to improve the estimation performance
- The global slope and strain were additionally considered as target responses
- The shape function and loss for slope and strain were added in the network, and the scaling process for this network was introduced to relieve the scale difference between responses
- Estimation target was limited to the static responses generated by random point live load in this study
- The responses generated by dead load were considered only to determining initial state of the cable-stayed bridge

The effectiveness of the extended algorithm was verified using an FEM model of a cable-stayed bridge. The effect of adding slope and strain data was analyzed by comparing the extended algorithm with the original algorithm developed by Byun and Kang (2023). In addition, the estimation performance of the proposed method was verified through a comparative study using SRALMR. Furthermore, the effect of the scale factor on the estimation performance was analyzed.

2. Methodology

In this section, the previously developed SRALMR and the proposed method based on an ANN are introduced. SRALMR estimates global deformation and internal forces using SSM and the least-squares method. As mentioned in the Introduction, the least-squares method is limited in that the optimization can be conducted only at the points where the measurement data are extracted. To overcome this limitation and improve the estimation performance, Byun and Kang (2023) implemented an ANN to enhance the method, but they used only displacement data for estimation. Therefore, in this study, the estimation method based on an ANN was extended to combine displacement, slope, and strain data, thus improving the estimation performance.

2.1 SRALMR

SRALD, which can estimate global deformations and internal forces, was developed by Choi *et al*. (2017b) and extended to SRALMR by Byun *et al*. (2022). While SRALD uses only displacement data, SRALMR uses a combination of displacement, slope, and strain data. Both SRALD and SRALMR are based on SSM and the least-squares method. In a linear system, each structural response can be represented as a product of the shape function Φ and the shape factor α. In addition, equal weight factors can be applied to the displacement u, slope θ, and strain ϵ responses owing to the mechanical relationship between the three responses. The slope and strain are, respectively, the first and second derivatives of the displacement. Consequently, the displacement, slope, and strain can be represented as shown in Eqs. (1)-(3).

$$\{u\} = [\Phi_u]\{\alpha\} \tag{1}$$

$$\{\theta\} = [\Phi_\theta]\{\alpha\} = [\Phi_u]'\{\alpha\} \tag{2}$$

$$\{\epsilon\} = [\Phi_\epsilon]\{\alpha\} = [\Phi_u]''\{\alpha\} \tag{3}$$

Eqs. (4)-(6) represent the i^{th} shape function for displacement $\Phi_{i,u}$, slope $\Phi_{i,\theta}$, and strain $\Phi_{i,\epsilon}$. The shape function for each response consists of the responses of all the degrees of freedom (DOF) considered in the analysis. Consequently, the i^{th} total shape function Φ_i presented in Eq. (7) corresponds to the combination of all shape functions in one matrix.

$${\Phi_{i,u}}^T = \left[u_{i1}\ u_{i2}\ u_{i3}\ u_{i4}\ \cdots\ u_{iN_{dof,u}}\right], \tag{4}$$

$${\Phi_{i,\theta}}^T = \left[\theta_{i1}\ \theta_{i2}\ \theta_{i3}\ \theta_{i4}\ \cdots\ \theta_{iN_{dof,\theta}}\right] \tag{5}$$

$${\Phi_{i,\epsilon}}^T = \left[\epsilon_{i1}\ \epsilon_{i2}\ \epsilon_{i3}\ \epsilon_{i4}\ \cdots\ \epsilon_{iN_{dof,\epsilon}}\right], \tag{6}$$

$$\Phi_i = \begin{bmatrix}\Phi_{i,u}\\ \Phi_{i,\theta}\\ \Phi_{i,\epsilon}\end{bmatrix}\ \left(N_{dof} \times 1\right), \tag{7}$$

where $N_{dof} = N_{dof,u} + N_{dof,\theta} + N_{dof,\epsilon}$ is the total number of DOF; $N_{dof,u}$, $N_{dof,\theta}$, and $N_{dof,\epsilon}$ are the number of displacement, slope, and strain DOF, respectively; and $u_{iN_{dof,u}}$, $\theta_{iN_{dof,\theta}}$, and $\epsilon_{iN_{dof,\epsilon}}$ represent the displacement, slope, and strain values at each DOF in the i^{th} shape function, respectively.

As previously mentioned, the global structural response can be represented as the product of the shape function and the shape factor. To establish the error function, an arbitrary response shape $\widetilde{ARS}$ needs to be defined, as shown in Eq. (8), which can be transformed into matrix form, as displayed in Eq. (9). The matrix size of $\widetilde{ARS}$ is $(N_{dof} \times 1)$.

$$\begin{aligned}\widetilde{ARS} &= \alpha_1\Phi_1 + \alpha_2\Phi_2 + \alpha_3\Phi_3 + \cdots + \alpha_{N_{sf}}\Phi_{N_{sf}}\\ &= \sum_{i=1}^{N_{sf}} \alpha_i\Phi_i,\end{aligned} \tag{8}$$

$$\widetilde{ARS} = \left[\Phi_1\ \Phi_2\ \Phi_3\ \cdots\ \Phi_{N_{sf}}\right]\begin{bmatrix}\alpha_1\\ \alpha_2\\ \alpha_3\\ \vdots\\ \alpha_{N_{sf}}\end{bmatrix} \tag{9}$$

where N_{sf} is the number of shape functions.

While $\widetilde{ARS}$ includes arbitrary response values at each DOF, the measurement data matrix consists of actual displacement ω, slope ∅, and strain ε response values measured at the specific positions where sensors are installed. Consequently, the total measurement data matrix MD is established by combining MD_ω, $MD_\emptyset$, and $MD_{\boldsymbol{\varepsilon}}$ into one matrix as shown in Eqs. (10)-(13).

$${MD_\omega}^T = \left[\omega_1\ \omega_2\ \omega_3\ \omega_4\ \cdots\ \omega_{N_{md,\omega}}\right] \tag{10}$$

$${MD_\emptyset}^T = \left[\emptyset_1\ \emptyset_2\ \emptyset_3\ \emptyset_4\ \cdots\ \emptyset_{N_{md,\emptyset}}\right] \tag{11}$$

$${MD_\varepsilon}^T = \left[\varepsilon_1\ \varepsilon_2\ \varepsilon_3\ \varepsilon_4\ \cdots\ \varepsilon_{N_{md,\varepsilon}}\right] \tag{12}$$

$$MD = \begin{Bmatrix}MD_\omega\\ MD_\emptyset\\ MD_\varepsilon\end{Bmatrix}\ \left(N_{md} \times 1\right), \tag{13}$$

where N_{md} is the number of measurement data points.

To establish the error function using MD and $\widetilde{ARS}$, it is necessary to extract arbitrary response values from $\widetilde{ARS}$ only at the DOF where measurement data exists. Therefore, $\widetilde{ARS}$ is adjusted to ARS, and the error function E is established as the sum of the square error between MD and ARS as shown in Eq. (14). The optimal shape factor for minimizing the error can be defined as the shape factor that makes the partial differential equation of E equal to zero. The calculation process is represented by Eqs. (15)-(17), where Eq. (17) is a representative estimation equation widely used in various studies based on SSM and the least-squares method.

$$E = \sum_{j=1}^{N_{md}} \left(MD_j - ARS_j\right)^2 \tag{14}$$

$$\frac{\partial E}{\partial \alpha_k} = 2\sum_{j=1}^{N_{md}} \left[\left(MD_j - ARS_j\right)\left(\frac{\partial MD_j}{\partial \alpha_k} - \frac{\partial ARS_j}{\partial \alpha_k}\right)\right] = 0 \tag{15}$$

where $k = 1, 2, \cdots N_{sf}$

$$\begin{aligned}\frac{\partial E}{\partial \alpha_k} &= \sum_{j=1}^{N_{md}} \left[\left(\sum_{i=1}^{N_{sf}} \alpha_i \Phi_{ij}\right)\left(\Phi_{kj}\right)\right] \\ &= \sum_{j=1}^{N_{md}} \left[\left(MD_j\right)\left(\Phi_{kj}\right)\right]\end{aligned} \tag{16}$$

where $k = 1, 2, \cdots N_{sf}$

$$\begin{aligned}&[\Phi]^T_{N_{md}\times N_{sf}}[\Phi]_{N_{md}\times N_{sf}}\{\alpha\}_{N_{sf}\times 1} \\ &= [\Phi]^T_{N_{md}\times N_{sf}}\{MD\}_{N_{md}\times 1}\end{aligned} \tag{17}$$

From Eq. (17), the optimal shape factor can be calculated using an inverse matrix of $[\Phi]^T[\Phi]$. However, $[\Phi]^T[\Phi]$ becomes a rank-deficient matrix if N_{sf} is greater than N_{md}. In this case, the singular value decomposition (SVD) method can be alternatively used to calculate the shape factor. Subsequently, each global structural response can be estimated by substituting the derived shape factor into Eqs. (1)-(3). In addition, global internal forces such as the axial force and bending moment can be determined using the estimated global strain.

2.2 Proposed method

Although the least-squares method has been widely adopted to minimize the error between the estimated and measured data, it has the limitation of minimizing only the error at the measurement points. To overcome such a limitation, Byun and Kang (2023) introduced an estimation method based on an ANN using displacement data. However, it is difficult to directly measure the displacement using conventional displacement meters and GNSS receivers are expensive to install at multiple locations. Therefore, in this study, the estimation method introduced by Byun and Kang (2023) was extended to use a combination of displacement, slope, and strain data. Slope and strain responses were additionally considered in input variables and estimation target. To achieve the aim of this study, the shape function and loss for slope and strain were also added in the network. In addition, the scaling method for this network was proposed to minimize the error due to the scale difference between responses. The extension of the estimation method can improve the accuracy and reduce the cost of SHM systems.

The estimation of global responses using limited response data is the regression problem. For the regression problem, various machine learning algorithm such as support vector machine (SVM), DT, RF, and ANN can be used. SVM is a powerful algorithm for both classification and regression tasks, known for its ability to handle high-dimensional data and capture nonlinear relationship using kernel functions (Cortes and Vapnik 1995). DT are intuitive and offer transparency in their decision-making process and RT is an ensemble method that combines multiple DTs to enhance performance and reduce overfitting (Breiman 2001). While these traditional machine learning algorithms have their own strengths, ANN offers enhanced predictive capabilities when the pattern is intricate and data is massive due to multi-layer architecture. In this study, the algorithm that can capture the complex relationship between responses was required and numerous data was generated by numerical analysis. Therefore, ANN is adopted to establish the estimation algorithm for performance improvement.

The basic idea of the algorithm extension lies in the differential relationship between the responses. As explained in section 2.1, the same shape factor can be applied to all responses due to their differential relationship. Therefore, the network can be established considering the shape factor as the output and the measured displacement, slope, and strain data as the multiple inputs. The idea of using the same shape factor is identical to that of SRALMR, but there are two major differences: the target of error minimization and the consideration of the relationship between measured data. First, while the least-squares method minimizes the error only at the measurement positions, the proposed network minimizes the error at all DOFs considered in the analysis. Second, the relationship between all measurement data is considered by the weights and biases of the multi-input network. These differences in the proposed method can improve estimation performance.

Fig. 1 shows the architecture of the proposed method based on an ANN. The network consists of an input layer, two hidden layers, an output layer, and a post-calculation process. All the measurement data were included in the input layer, and the shape factor was derived at the output layer. Therefore, the sizes of the input and output layers were fixed at N_{md} and N_{sf}, respectively. Because a 2D cable-stayed model was used in this study, responses in terms of horizontal and vertical displacement, longitudinal slope, and strain were used in the network. The size of hidden layer, the number of hidden layer, loss function were determined through the optimization process. A leaky ReLu was adopted as the activation function to prevent exploding, vanishing, and knock-out problems. In the post-calculation process, the global horizontal displacement U1, vertical displacement U2, slope UR, and strain E were calculated by multiplying the derived shape factor by the shape function of each response. The total loss was then taken as the sum of the losses of each response. Another important factor is the scale difference between responses. The scale factor sf must be applied to the estimation performance because the responses have a different value range. In this study, the scale factor for each response based on the vertical displacement is derived using the shape function, as shown in Eq. (18). The scale factor is applied to the input for improving the training performance and to the loss for adjusting the impact of each response on the estimation. Finally, the deformation was determined by the estimated

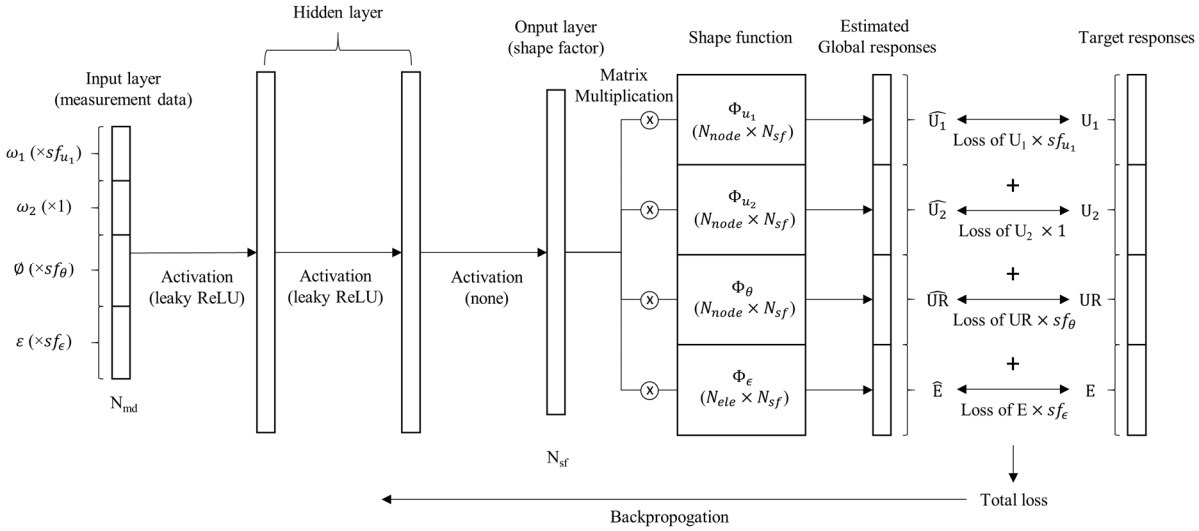

Fig. 1 Architecture of the ANN proposed for estimating global responses

global horizontal and vertical displacements, and the internal forces were calculated using the estimated global strain.

$$sf = \frac{\text{mean}\left[\max(|\Phi_1|), \max(|\Phi_2|), \max(|\Phi_3|), \cdots, \max\left(\left|\Phi_{N_{sf}}\right|\right)\right]}{\text{mean}\left[\max\left(\left|\Phi_{1,u_2}\right|\right), \max\left(\left|\Phi_{2,u_2}\right|\right), \max\left(\left|\Phi_{3,u_2}\right|\right), \cdots, \max\left(\left|\Phi_{N_{sf},u_2}\right|\right)\right]} \tag{18}$$

3. Target model and data generation

A radiating-type cable-stayed bridge was adopted as the target model to apply and validate the method proposed in this study. The shape function required for the estimation of the structural responses is derived through a static analysis of the target model. In addition, the data required for training, validating, and testing the network were generated by combining the shape functions. Details of the target model, shape function, and data generation are described below.

3.1 Target numerical model

Because the main objective of this study is to validate the performance improvement of the proposed method compared with previous methods, the synthetic cable-stayed bridge introduced by Kim *et al*. (2016a) was adopted as target numerical model. In addition, this model has been used to evaluate nonlinear characteristics (Kim *et al*. 2016b) and estimate global responses through SRALMR (Byun *et al*. 2022).

Fig. 2 shows the numerical model of the target cable-stayed bridge, which consists of a 3-span girder, two pylons, and forty cables. The total length and height were 920 and 160 m, respectively. The bottom of the pylons was fixed and both sides of the girder were roller-supported. At the intersections of the pylons and girder, roller supports were applied only to the girder to free it in the longitudinal direction. The circular markers in Fig. 2 indicate the locations where the measurement data were extracted for each response, corresponding to points where each response value was generally large. Fig. 3 shows the cross-sections of the girder and pylons. Note that the shape of the cross-section does not directly affect the structural responses in the 2D beam model. Only the material and geometric

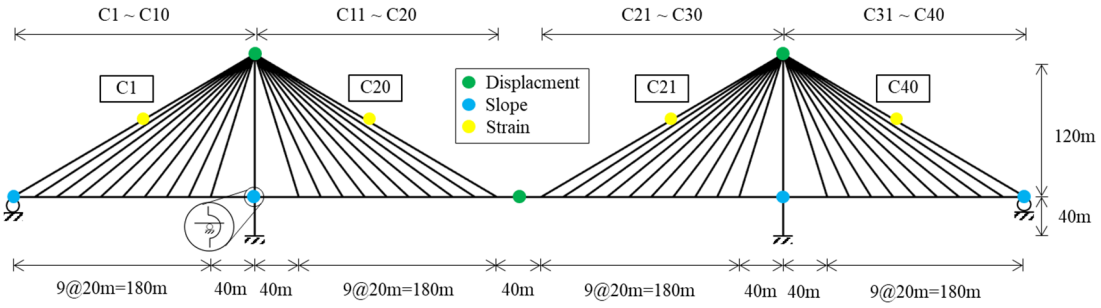

Fig. 2 Specifications of target model and extraction points of measurement data

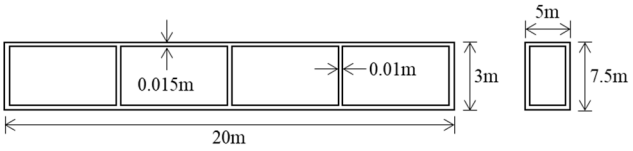

Fig. 3 Cross-sections of the girder (left) and pylons (right)

Table 1 Material and properties of main members

Properties	Girder	Pylon	Cable
Elastic modulus (kN/m^2)	2.1×10^8	2.1×10^8	2.1×10^8
Sectional area (m^2)	0.749	0.374	0.02
2nd moment of inertia (m^4)	1.446	3.143	-
Unit weight (kN/m^3)	222.72	78.50	78.50

properties provided in Table 1 affect the responses. The additional weight of ancillary components such as barriers and pavement was considered in unit weight of girder. The numerical model was implemented in Abaqus 2022. The girder and pylons and cables were modeled as beam and truss elements, respectively. The number of nodes on the girder and each pylon was 47 and 9, respectively. The first three frequencies of the target model derived from the frequency analysis are 0.258 Hz, 0.368 Hz, and 0.657 Hz.

3.2 Initial state analysis and model validation

In the design of the cable-stayed bridge, deformation under the dead load are controlled by the pre-tension force of the cables. In addition, pre-tension of the cables significantly affect the stiffness of the structure. Therefore, optimal initial state under the dead load should be considered to derive the rational structural responses from the numerical model. In this study, the initial force method was adopted to determine the initial equilibrium state of the target model. In the initial force method, the process involves iteratively considering the current iteration's internal forces of all members as initial internal forces in the subsequent iteration. This initial state analysis is iteratively performed based on the nonlinear FE analysis until the deformation is under tolerance. The displacements of girder center and pylon top were represented in Fig. 4. It is shown that the displacement converges as the iteration progresses.

In addition, to validate the numerical model, final cable pre-tension forces of this study was compared with that of Kim *et al*. (2016a) in Fig. 5. The result shows that the pre-tension forces of this study are good agree with that of Kim *et al*. (2016a). The slight error of tensile forces occurred due to the slight difference in unit weight and initial tension force of the iteration process.

As mentioned above, initial state of the main members significantly affects the structural responses. Therefore, all responses for estimation were derived by applying live load after initial state analysis. In real completed structure, however, it is hard to measure the response at the initial state. Therefore, only the response excluding the initial state response from the final response was determined as the estimation target. If the structure behaves in the linear

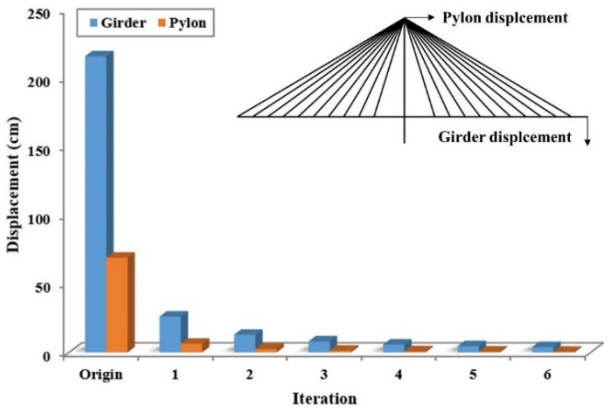

Fig. 4 Displacements of girder and pylon in each iteration of initial state analysis

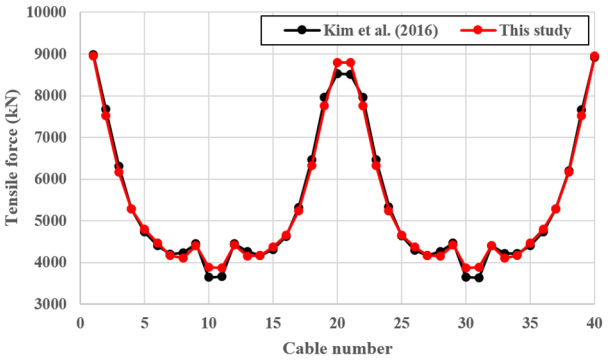

Fig. 5 The final pre-tension force of the cables determined through the initial state analysis

range, the final response can be easily obtained as the sum of the initial state response and the estimated response.

3.3 Shape function

The shape function was used for estimating the structural response based on the SSM. In previous studies, various shape functions have been suggested and applied. Theoretical shapes, such as the sine function, power series, the mode shape derived from frequency analysis, and the structural shape function (SSF), can be utilized as the shape function. The SSF can be derived by sequentially applying a unit load to all the nodes of the numerical model where loads can occur. Estimation using mode shape showed better performance than that using theoretical shapes because structural characteristics were included (Cho *et al*. 2015). Byun *et al*. (2022) reported that SSF can estimate structural responses for static systems more accurately than mode shape because SSF represents the response shape derived by directly applying a load to the target model. Therefore, in this study, an SSF derived by sequentially applying a load to the girder in the vertical direction was adopted as the shape function. A load of 1000 kN was used to reduce the estimation error due to the scale difference with the target model. The number of shape functions was equal to the number of nodes in the girder.

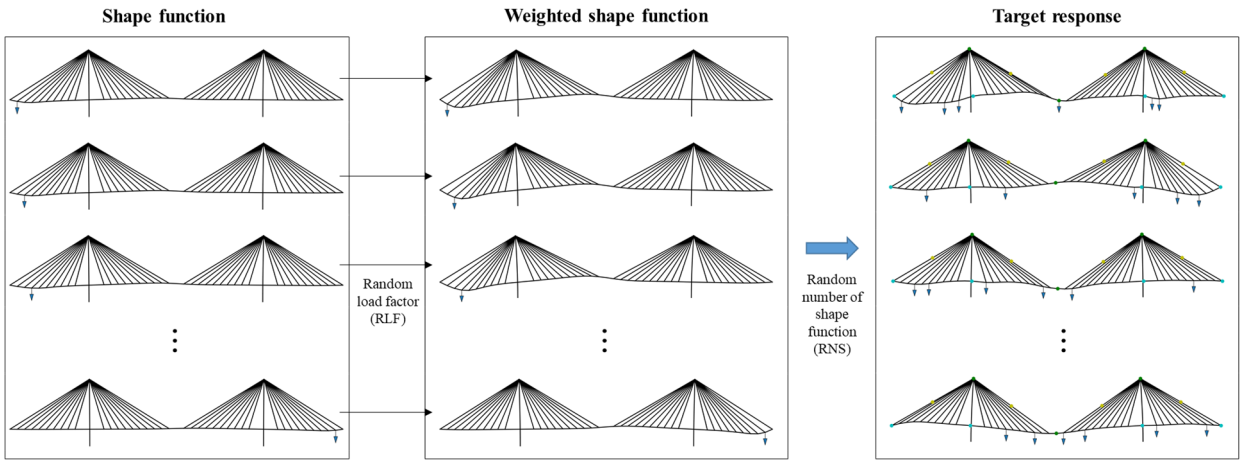

Fig. 4 Data generation process using shape function

Table 2 Specifications of datasets

Data type	Training	Validation	Testing
Sets	10,000	3,000	3,000
RLF	1, 2, 3, 4	1.5, 2.5, 3.5	5, 6, 7
RNS	1, 3, 5	2, 4	6, 7

3.4 Data generation

Because it takes a long time to generate sufficient data for network learning through numerical analysis, data were generated by combining several weighted shape functions through two processes as shown in Fig. 4. First, each shape function was weighted by multiplying by a random load factor (RLF). Second, each target datum is derived by combining a random number of weighted shape functions (RNS). The training, validation, and testing datasets were generated separately according to RLF and RNS. The specifications of the dataset are listed in Table 2. Although RLF and RNS for the validation dataset were defined in the range of the training dataset, those for the testing dataset were out of range for evaluating the general performance of the network. Training, validation, testing dataset contained 10,000, 3,000, and 3,000 sets of target global responses and measured data. These measured data were extracted from the target global responses at the measurement points, as shown in Fig. 2. The target and measured data included the displacement, slope, and strain responses.

4. Performance evaluation

This section describes the details of the proposed network, the effect of multi-response data, and the performance evaluation of the proposed method compared with SRALMR. First, the hyperparameters of the network, such as the learning rate and batch size, were determined. Second, the effect of multi-response data on the performance of the proposed method was analyzed by considering three cases of response data combination. The global displacement, slope, and strain were estimated using limited response data for each case and were compared with the target data. Finally, the estimation performance of the proposed method was validated by comparing it with that of SRALMR. The global deformation and internal forces (girder moments, girder section forces, and cable forces) were estimated and used to evaluate performance. Internal forces were derived using the estimated global strain. Fig. 5 shows a flowchart of the entire process for both the proposed method and SRALMR, including data generation, algorithm execution, and performance evaluation.

The metrics used to evaluate the network performance for test dataset are normalized mean absolute percentage error (NMAPE) and R-squared score (R^2). The equations of metrics are represented in Eqs. (18) and (19). The data number n indicates the node number in the case of the displacement and slope and the element number in the case of the strain. y_i, and $\hat{y}_i$ are the i^{th} target and estimated values, respectively. $\bar{y}$ *and* y_{max} are the mean and maximum of the target values, respectively.

$$\text{NMAPE} = \frac{100}{n}\sum_{i=1}^{n}\frac{|y_i - \hat{y}_i|}{y_{max}} \tag{18}$$

$$R^2 = 1 - \frac{\sum_{i=1}^{n}(y_i - \hat{y}_i)^2}{\sum_{i=1}^{n}(y_i - \bar{y})^2} \tag{19}$$

4.1 Details of the network and hyperparameter tuning

An overview of the proposed network and data generation is presented in sections 2.2 and 3.3, respectively. Therefore, in this section, the details of the network layers and hyperparameters are determined, as shown in Tables 3. The sizes of the input and output layers were fixed at N_{md} and N_{sf}, respectively. The size of all hidden layers are the same. A leaky ReLu is adopted as the activation function and applied to all layers except the output one. The Adam optimizer was applied and the initial learning rate was 0.001. In addition, learning rate scheduler and early stopping modules was additionally applied to prevent overfitting. Early-stopping patience, scheduler patience, and

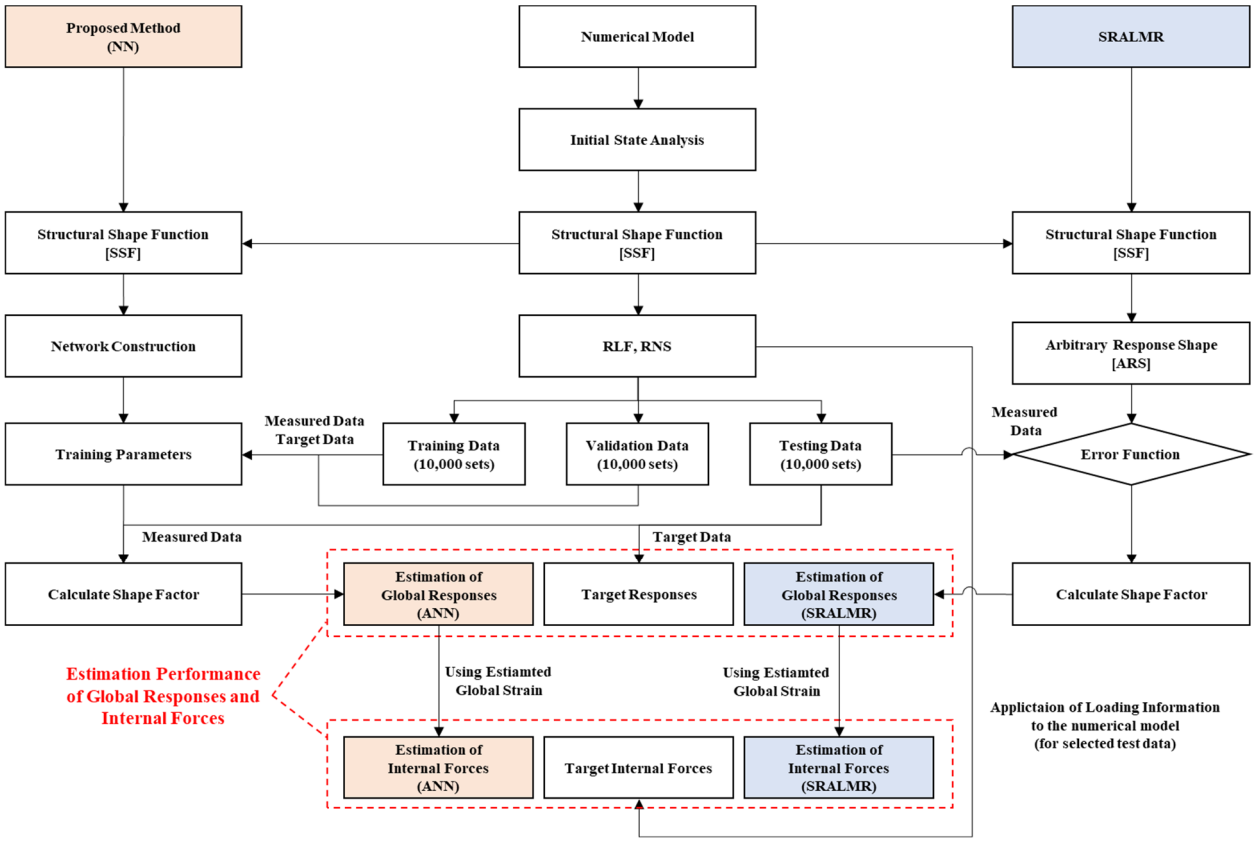

Fig. 5 Flowchart of the proposed method compared with that of SRALMR

Table 3 Specifications of the hyperparameters

Hyperparameter	Value (candidates)
Hidden size	500 (50, 100, 200, 500, 1000)
Hidden layer number	2 (1, 2, 3)
Loss function	MAE (MSE, MAE)
Optimizer	Adam
Learning rate	0.001
Batch size	32
Patience (early-stop)	20
Patience, epsilon (scheduler)	10, 0.0001

Table 4 Estimation performance for test dataset according to the hyperparameter

Hidden size	Hidden layer number	Loss function	Training time (min.)	NMAPE (%)	R^2
50	2	MAE	18.82	2.23	0.972
100	2	MAE	10.76	1.94	0.976
200	2	MAE	9.53	1.89	0.978
500	2	MAE	8.63	1.94	0.978
1000	2	MAE	7.72	1.98	0.978
200	1	MAE	21.86	2.11	0.973
200	3	MAE	10.55	1.93	0.978
200	2	MSE	9.88	2.37	0.978

scheduler epsilon are 20, 10, and 0.0001. For other hyperparameters (hidden size, hidden layer number, and loss function), tuning was performed for case of using all 14 measurement data. The hyperparameter candidates are shown in Table 3 and the estimation performance according to the hyperparameter is represented in Table 4. Through the hyperparameter tuning, determined hidden size, hidden layer number, and loss function were 500, 2, and MAE, respectively.

4.2 Effect of multi-response data

The major enhancement of the proposed algorithm is the use of a combination of displacement, slope, and strain responses to improve the estimation accuracy and reduce the need for high-cost GNSS. Therefore, in this section, the effect of different combinations of the multi-response data is analyzed. Three combinations were considered in the analysis: three displacement data (Case 1), three displacement and four slope data (Case 2), and three displacement, four slope, and four strain data (Case 3). The displacement data included horizontal and vertical displacements. The extraction locations for each response are shown in Fig. 2. For all cases, only the loss of the responses included in the input was considered when training the network. For example, the losses of displacement and slope were considered in Case 2. In addition, the sum of the considered losses was taken as the total loss due to backpropagation. Case 1, which used only displacement data, is the method proposed by Byun and

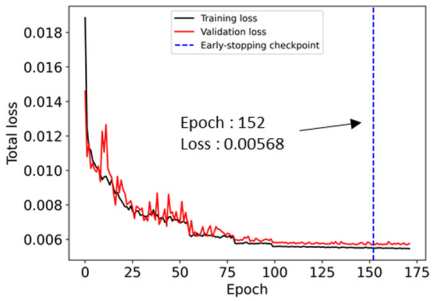

(a) Case 1

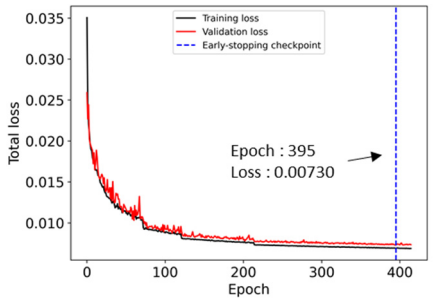

(b) Case 2

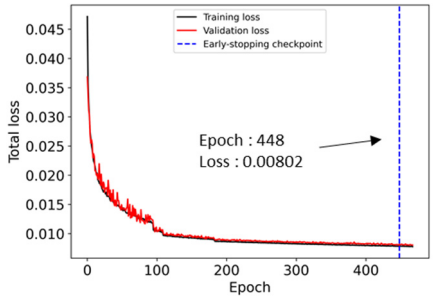

(c) Case 3

Fig. 6 Training and validation losses for each case according to the epoch

Kang (2023). Case 2 and Case 3, which additionally used slope and strain data, is the extended method in this study.

Fig. 6 shows the epoch losses of the training and validation data for each case; the epoch and loss values at the early-stopping checkpoint are included. The general trend observed from the losses in all cases was a sharp decrease at the beginning of learning and a similar loss between training and validation. However, there was a difference in the values of the epoch and loss at the converging point. The more response data used, the larger the epoch required for sufficient learning. The loss is also larger depending on the case because the loss is derived by the summation of losses for the considered responses. However, the loss in Case 3 is smaller than that in Case 2. To analyze the loss trend in detail, the validation loss for each response according to the case is presented in Table 5. Although the improvement in the estimation of horizontal displacement is small owing to its small variability according to the target data, the loss of vertical displacement and slope considerably decreases as the response is added. Comparing Cases 2 and 3, although the loss for strain is added, the total loss decreased because the loss of vertical displacement and slope was significantly reduced.

Table 5 Validation loss of each response according to the case

Case	U1	U2	UR	E
Case 1	0.000739	0.004941	-	-
Case 2	0.000507	0.002051	0.004740	-
Case 3	0.000343	0.001193	0.003115	0.003370

Table 6 Average estimation error for the test dataset according to the case

Case	NMAPE (%)	R^2
Case 1 (Byun and Kang 2023)	4.430	0.880
Case 2 (This study)	2.713	0.959
Case 3 (This study)	1.887	0.978

After training, the trained network was applied to test dataset to evaluate the estimation performance. Table 6 shows the average estimation error of all responses for the test dataset according to the case. From the results, it is indicated that the proposed algorithm additionally considering slope and strain data showed better performance than the algorithm proposed by Byun and Kang (2023). To analysis estimation performance for each response, the box-plot of NMAPE and R^2 score were shown in Figs. 7-8, respectively. Figs. 7(a) and 8(a) represents the average value of horizontal and vertical displacement, while Figs. 7(d) and 8(d) indicates the average value of all responses. For displacement, median estimation performance was similar, but the estimation error range of case 1 was larger than that of other cases. Whereas, additional consideration of slope and strain data resulted in significant performance improvement for estimating of global slope and strain.

4.3 Comparative study

In this section, a comparative study between the extended model and SRALMR is conducted to evaluate the estimation performance of the proposed method. A non-scaled ANN is also considered in the comparison to analyze the effect of the scale factor applied to each response. The non-scaled and scaled ANN were trained using the training and validation datasets. Next, each target response of the test dataset was estimated using the estimation method. Subsequently, three targets were selected from the probability density function (PDF) of the error difference between SRALMR and the proposed method to evaluate the estimation performance in detail. For the three selected targets, the global deformation and internal forces (girder moments, girder section forces, and cable forces) estimated by each method were compared and analyzed.

At the early-stopping checkpoint, the epoch and

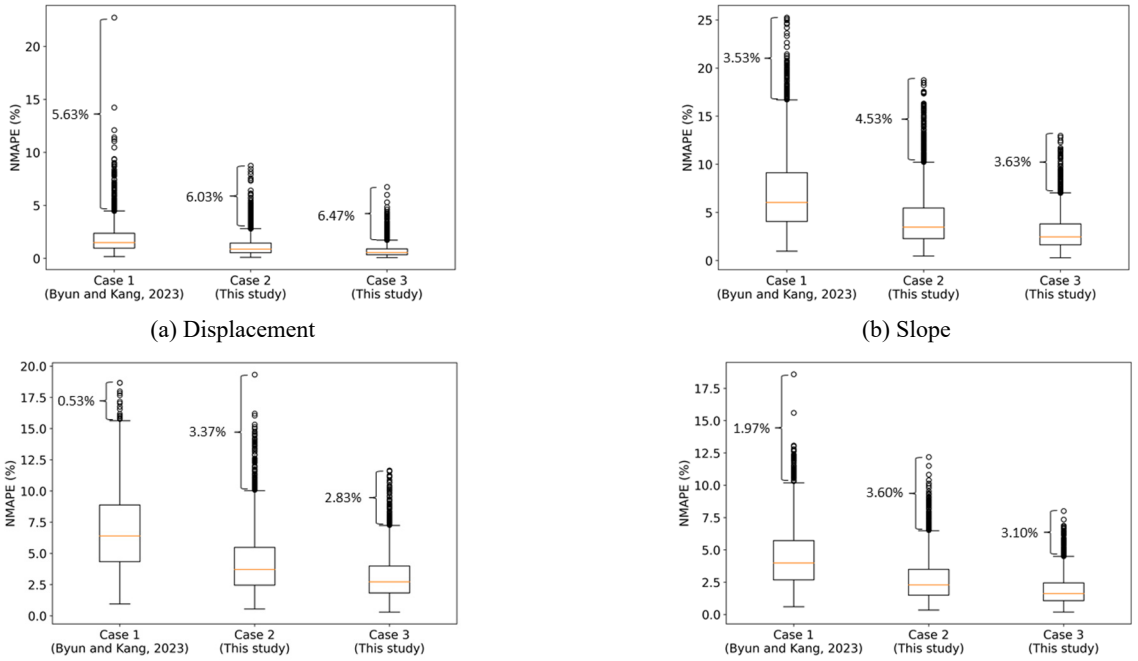

(a) Displacement (b) Slope

(c) Strain (d) Average

Fig. 7 Estimation error (NMAPE) of each response for each case when applying to test data

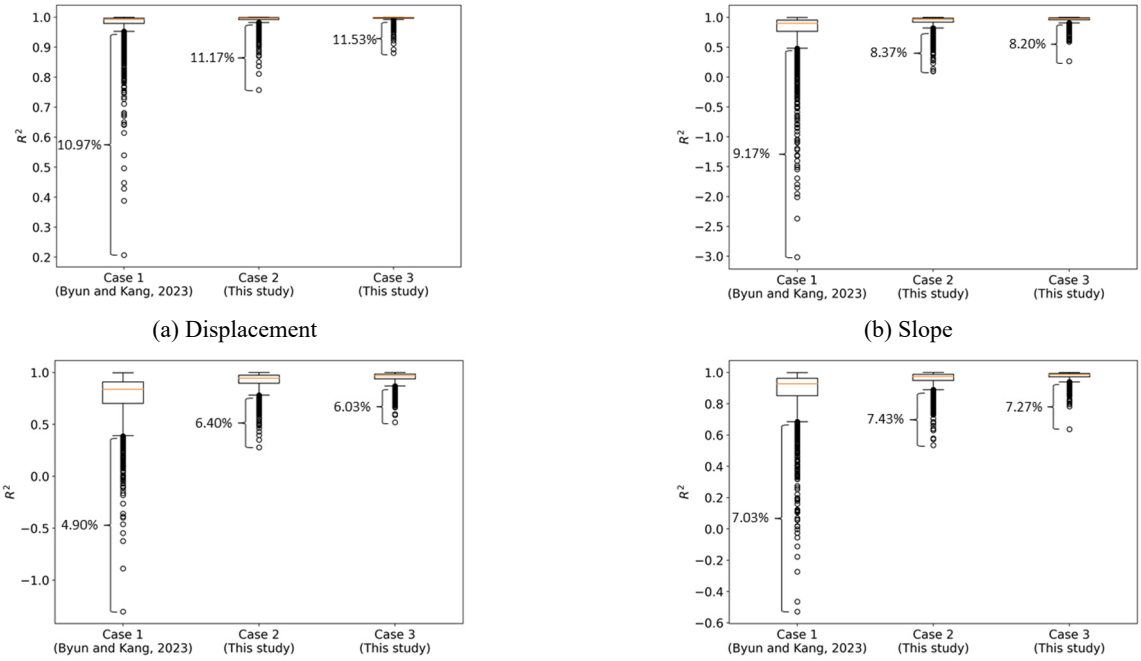

(a) Displacement (b) Slope

(c) Strain (d) Average

Fig. 8 Estimation error (R^2) of each response for each sensor layout case when applying to test data

validation losses were, respectively, 387 and 0.00642 for the non-scaled ANN, and 448 and 0.00802 for the scaled ANN. Owing to the scale factor for input and loss, the total loss and required epoch of the scaled ANN were larger than those of the non-scaled ANN. After completing the ANN training, the target responses of the test dataset were estimated using SRALMR, the non-scaled ANN, and the scaled ANN.

Figs. 9-10 show the NMAPE and R^2 score of each estimated response according to the estimation method. Figs. 9(d) and 10(d) indicate the average NMAPE and R^2 score for the displacement, slope, and strain. For all responses, the ANN method estimated the responses more accurately than SRALMR. The major difference between the ANN and SRALMR methods is that the former considers the relationship between the measured data of

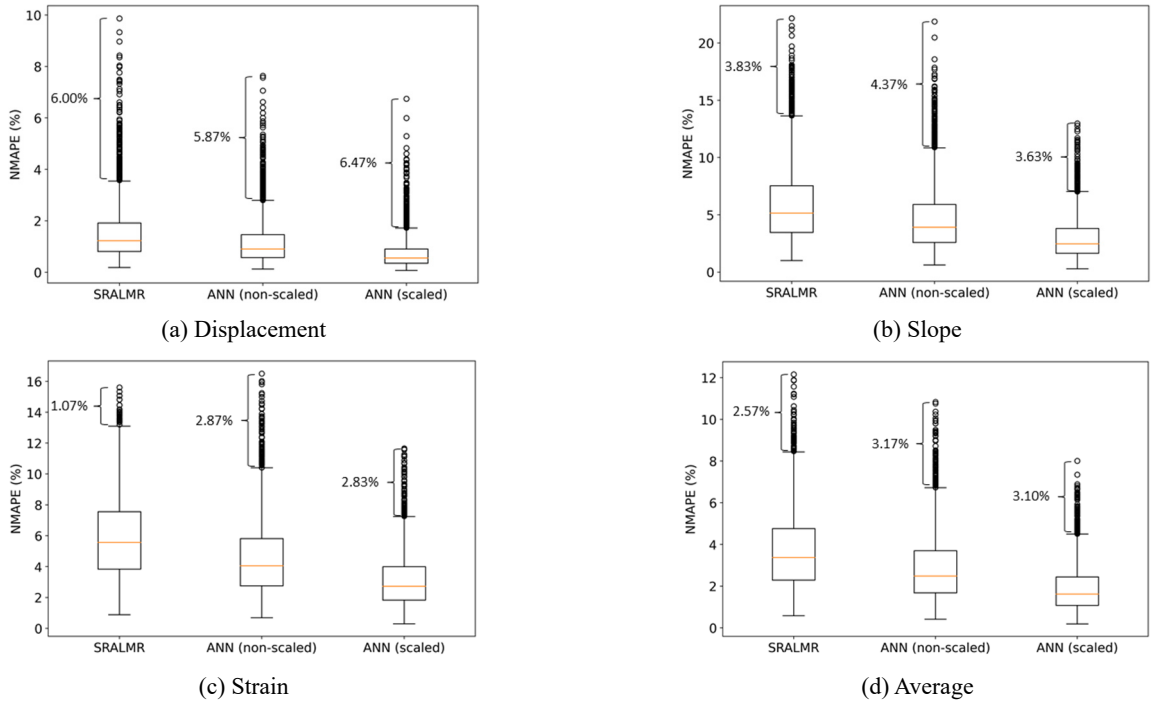

(a) Displacement (b) Slope

(c) Strain (d) Average

Fig. 9 Estimation error (R^2) for each response of test data according to the estimation method

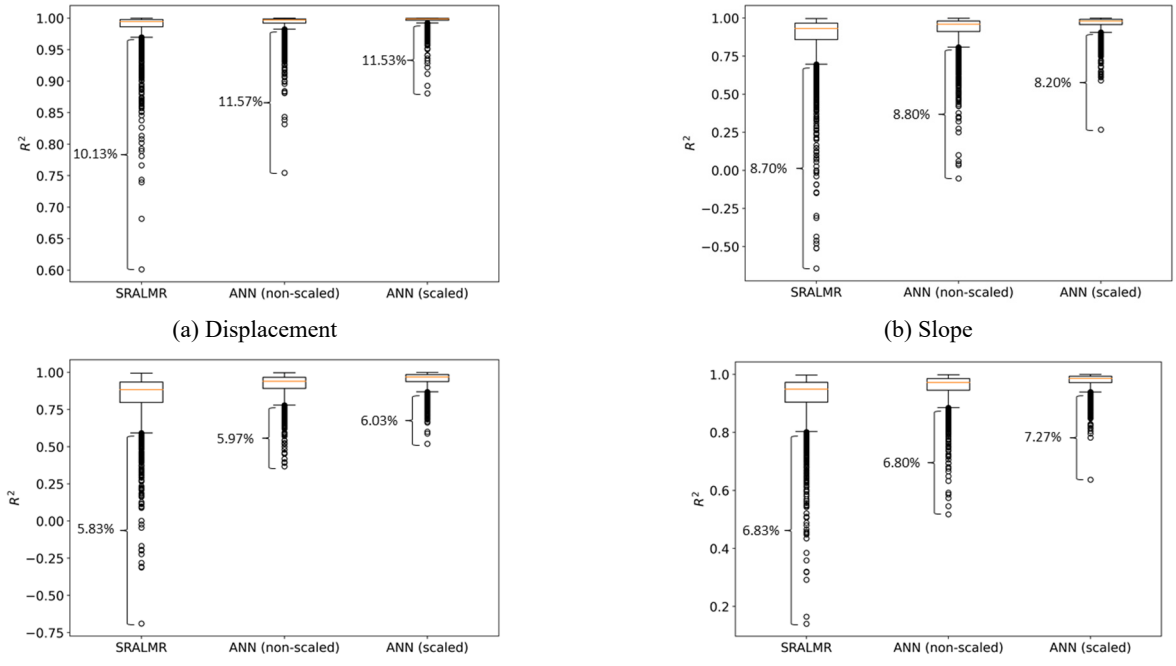

(a) Displacement (b) Slope

(c) Strain (d) Average

Fig. 9 Estimation error (NMAPE) for each response of test data according to the estimation method

each response and optimizes the estimation error for all the DOFs of the target model. For these reasons, the estimation method based on ANN shows a better performance than SRALMR. Comparing the non-scaled and scaled ANNs, the NMAPE of the latter was lower than that of the non-scaled ANN. This is because the losses for slope and strain with a relatively small scale compared to the vertical displacement are not sufficiently considered in the non-scaled ANN. Therefore, the decrease in the estimation error was larger for the slope and strain than for the displacement. Finally, the average NMAPE in Fig. 9(d) also show the same trend in the estimation error, being greater for SRALMR, intermediate for the non-scaled ANN, and lower for the scaled ANN. In addition, the outliers of the scaled ANN comprised only 3.10% of the total test dataset. It can be noted that ANN shows the best performance for the R^2

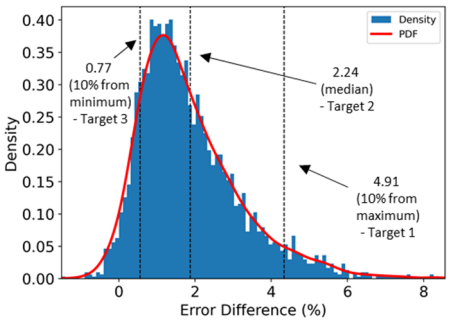

Fig. 11 NMAPE density of error difference between scaled ANN and SRALMR

score, similar to NMAPE. These results demonstrate that the scale factor is an essential component of the proposed method, making the scaled ANN a better estimation method than SRALMR.

Although the superior accuracy of the proposed method has been demonstrated, the previous results cannot sufficiently demonstrate the improvement of the proposed method for global response estimation. Therefore, three targets were selected from the PDF to analyze the global deformation and internal forces estimated by each estimation method in detail. A histogram of the estimation error difference between SRALMR and the scaled ANN is shown in Fig. 11. The PDF is derived using kernel density estimation, which is a non-parametric density estimation method that uses a kernel function. From the PDF, the probability that the error difference is greater than zero is 99.1%. This indicates that the scaled ANN exhibits a higher accuracy than SRALMR for more than 99% of the test dataset. In addition, three points (target 1: 10% from the minimum, target 2: median, and target 3: 10% from the maximum) were selected to analyze the estimation performance according to the error difference.

For the three selected targets, global deformation and internal forces (girder moments, girder section forces, and cable forces) were estimated using each method and compared to the target model, as shown in Figs. 12-14. For the deformation configuration, a scale factor was applied to clearly display the deformation. The loading and measurement extraction points are also shown in the deformed shape. The internal forces of the pylons are excluded from the analysis because they can be simply derived using the displacement at the top of each pylon. The internal forces for each element were derived using the estimated global strain, as shown in Eqs. (20)-(22).

$$SF_{girder} = E \times \left(\frac{\varepsilon_{top} + \varepsilon_{bottom}}{2}\right), \tag{20}$$

$$SM_{girder} = S \times E \times \left|\left(\varepsilon_{top} - \frac{\varepsilon_{top} + \varepsilon_{bottom}}{2}\right)\right| \tag{21}$$

$$SF_{cable} = E \times \varepsilon_{cable}, \tag{22}$$

where SF_{girder} and SM_{girder} are the section force and section moment of the girder, respectively, SF_{cable} is the section force of a cable, S is the section modulus, E is the elastic modulus, ε_{top}, ε_{bottom}, and ε_{cable} are the strains at the top of the girder section, at the bottom of the girder section, and across the cable section, respectively.

The estimated deformation and internal forces for target 1 with the largest error difference are shown in Fig. 12. In Fig. 12(a), the deformation estimated by SRALMR exhibits error at the girders of the second span. Because SRALMR uses a least-squares method that optimizes the estimation error only at measurement locations, the error can be large at unmeasured locations. Although the non-scaled ANN estimates the deformation more accurately than SRALMR, it is still less accurate than the scaled ANN, with the NMAPE of the non-scaled and scaled ANN being 1.30% and 0.24%, respectively. In Fig. 12(b) of the girder moment, the shape of the moment at the loading points and boundary conditions is sharp because the gradient of the moment changes rapidly at the points where concentrated loads are applied. The girder moment estimated by SRALMR does not sufficiently reflect this rapid change because shape superposition and the least-squares method result in a smooth line-based estimation between the points where measurement data exist. In other words, SRALMR cannot accurately estimate local rapid changes at non-measurement locations. In contrast, the proposed method can account for rapid local changes owing to the optimization method based on the ANN, which considers the losses for all DOFs in the target model. Therefore, the girder moments close to local points (such as girder numbers 13, 17, 27, and 34) are more accurately estimated based on the ANN than by SRALMR. Comparing the non-scaled and scaled ANN, although both can capture the rapid change in the girder moment, the values estimated by the scaled ANN are more accurate than those computed with the non-scaled ANN. The moment is directly related to the strain, and the accuracy of the estimated strain is significantly affected by the scale factor for strain loss. It has been previously demonstrated in Figs. 9(c) and 10(c) that the scaled ANN shows a higher estimation accuracy for strain than the non-scaled ANN. This is the reason for the difference in the girder moment estimation accuracy between the non-scaled and scaled ANN. Figs. 12(c) and (d) show, respectively, the girder section force and cable force estimated using each method. The girder section force of the cable-stayed bridge was determined from the girder axial strain and cable force. In addition, the cable forces were determined from the deformation of the girder and at the top of the pylons. Therefore, the cable forces estimated by SRALMD and the non-scaled ANN exhibited large errors in the second span. The estimation error in the cable forces leads to an estimation error in the girder-axial force.

Fig. 13 shows the target and estimated global responses for target 2, which resulted in the median error difference between SRALMR and the scaled ANN. Since the factors influencing estimation error are similar for all targets and target 1 was discussed earlier, only the trend of estimation performance for each method was described for targets 2 and 3. In Fig. 13(a), all methods estimate global deformation almost exactly, except for slight errors in the ranges of 300–400 m. For the girder moment in Fig. 13(b),

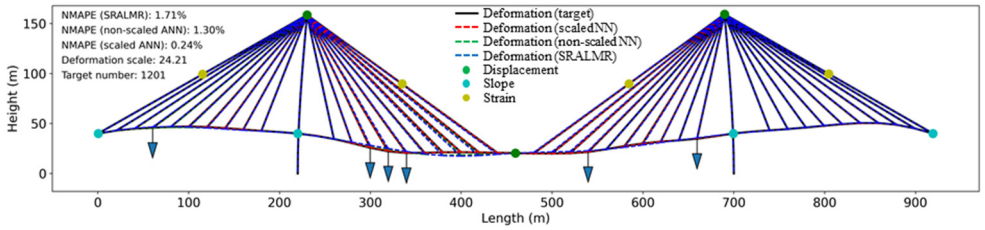

(a) Deformation

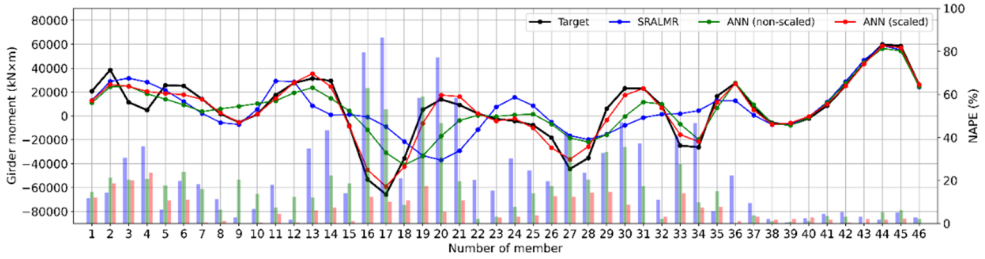

(b) Girder moments

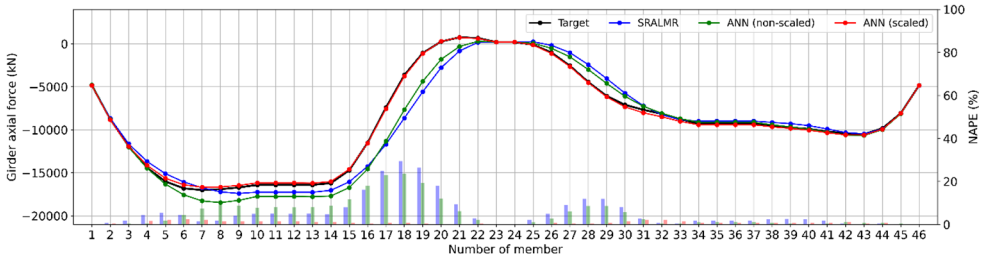

(c) Girder section forces

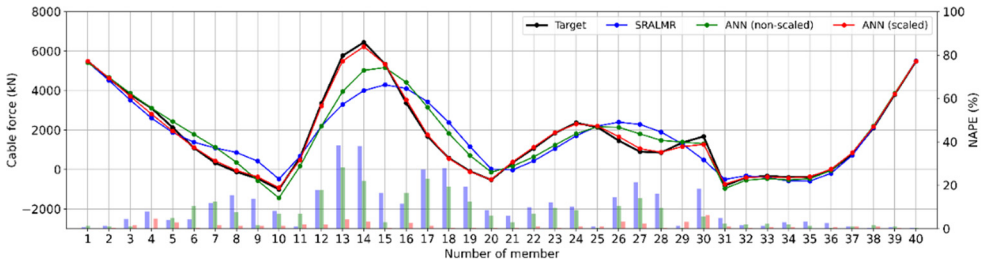

(d) Cable forces

Fig. 12 Estimated deformation and internal forces (target 1)

the rapid change in the moment is best estimated by the scaled ANN compared to SRALMR and the non-scaled ANN. As in the case of the moment, the scaled ANN showed the best estimation performance for the girder section forces and cable forces, as shown in Figs. 13(c)-(d).

Fig. 14 shows the target and estimated responses for target 3, which presented the lowest error difference. All methods estimate the global deformation and internal forces similarly because the response shapes of target 3 are relatively simple compared with those of targets 1 and 2. However, the limitations of the least-squares method and the scale factor effect are present in the estimation results, as in targets 1 and 2.

The estimation error for all estimated global responses according to the target is represented as NMAPE in Fig. 15, where DM is the deformation. All estimation methods estimate the global deformation within a 5% error, whereas a relatively large error occurs for global internal forces. This was because the internal forces were determined from the strain, and the strain shape exhibited a rapid gradient change near the loading points. Despite this difficulty in the estimation of global internal forces, the scaled ANN proposed in this study shows a more stable and accurate estimation performance than the SRALMR and non-scaled ANN.

5. Discussion and limitation

The aim of this study is to enhance the accuracy of estimating global deformation and internal forces by extending a previously developed method that utilized only displacement data. The extended method incorporates slope and strain data as additional input and incorporates loss

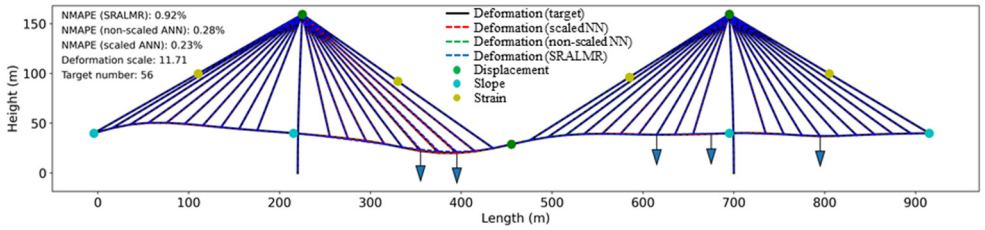

(a) Deformation

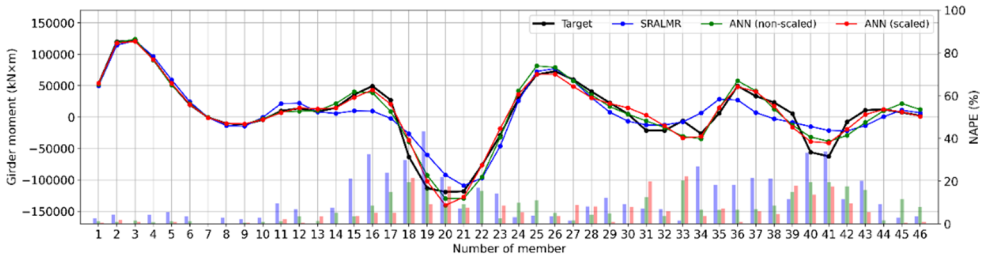

(b) Girder moments

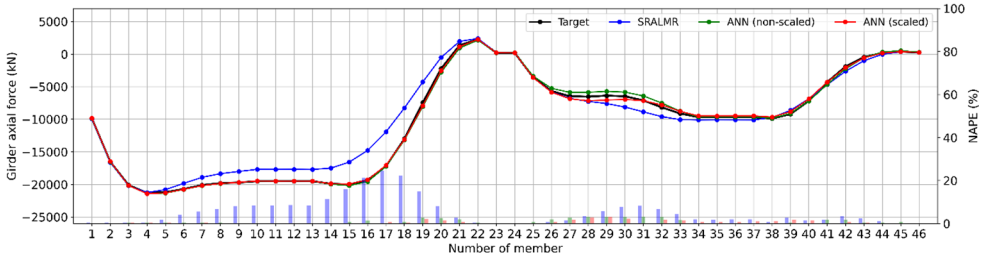

(c) Girder section forces

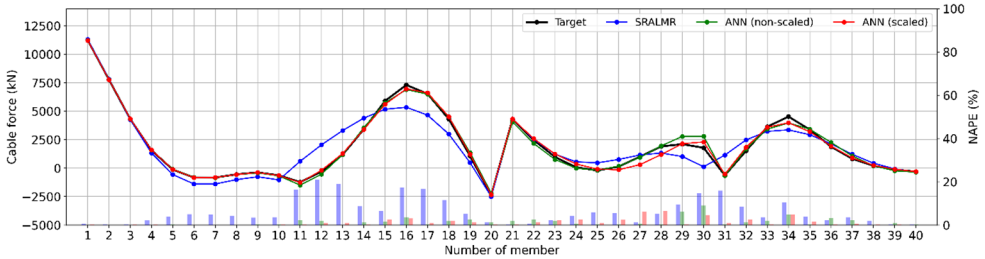

(d) Cable forces

Fig. 13 Estimated deformation and internal forces (target 2)

functions for each response to train the network. In Section 4.2, the effectiveness of the multi-response network is confirmed. The estimation results indicate that the inclusion of slope and strain data improves accuracy. In Section 4.3, the proposed method's performance is compared to that of SRALMR, which uses the least-squares method with multi-response data. The main difference between the proposed method and SRALMR lies in their optimization targets. While SRALMR minimizes the estimation error only at the measurement points, the proposed method minimizes the estimation error at all DOFs of the target structure. Consequently, the proposed method shows superior performance in estimating global responses compared to SRALMR, which cannot accurately estimate responses at points without input data and capture rapid local changes near the loading points. The proposed method overcomes this limitation using a neural network. Fig. 16 shows the SHM strategy using the proposed algorithm. The measurement data sequentially feed into the proposed algorithm. In addition, shape function derived from the FE model are included in the algorithm. Finally, sequential global internal forces can be estimated using shape function and sequential multi-response measurement data.

The deformation and internal forces estimated by the proposed method can be used to evaluate the structural integrity by comparing them with the deflection limit and nominal strength of each member suggested in various design specifications. However, the proposed neural network is based on a numerical model and only verified with static response data. Thus, future research will investigate applying the proposed method to real structures considering multiple loads moving randomly. First, we will study the application of the proposed method to dynamic data and combine it with the model updating method. Then, we will verify the proposed method with real structure data.

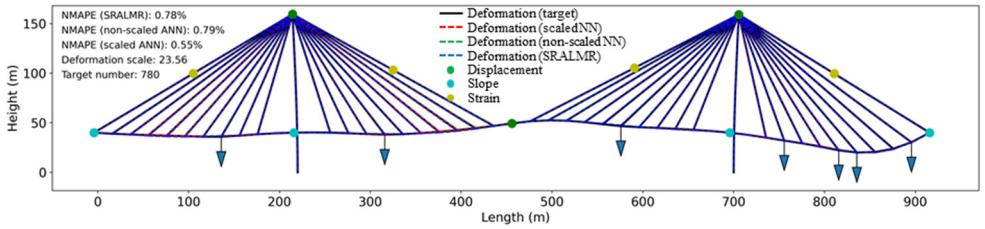

(a) Deformation

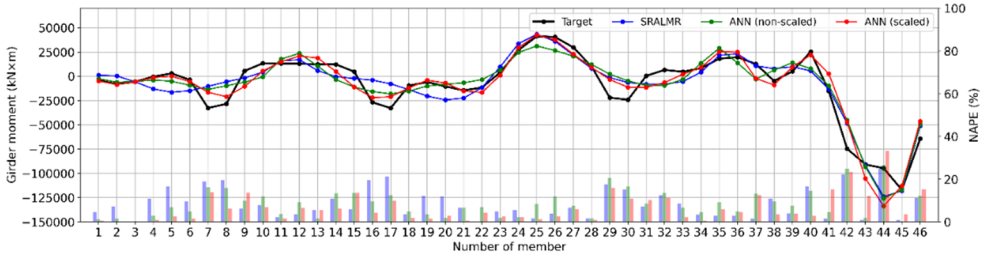

(b) Girder moments

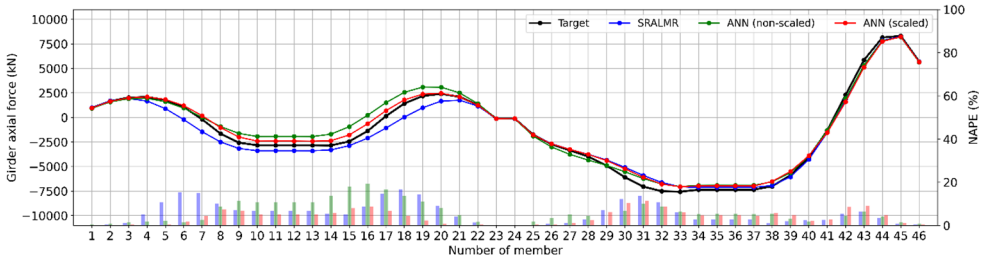

(c) Girder section forces

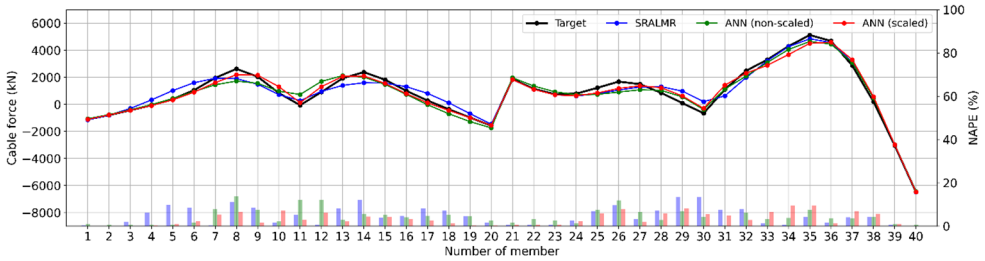

(d) Cable forces

Fig. 14 Estimated deformation and internal forces (target 3)

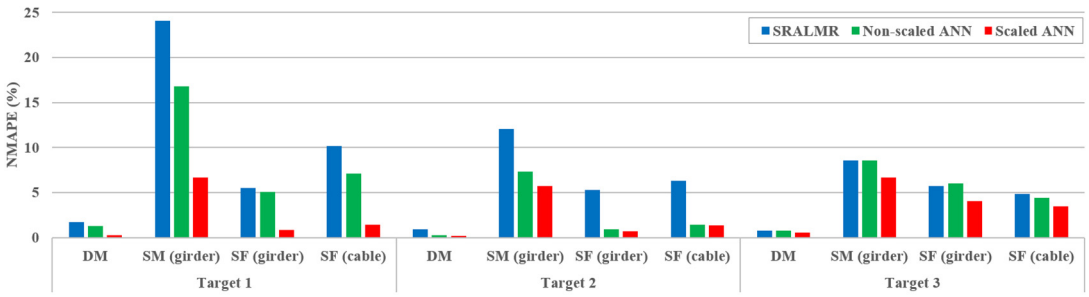

Fig. 15 NMAPE for all estimated global responses according to the target

6. Conclusions

In this study, a previously developed method for estimating global responses based on an ANN and the use of only displacement data was extended to combine displacement, slope, and strain data. The improvement of the proposed method was evaluated by analyzing the effects of inputting multi-response data. In addition, a comparative analysis with SRALMR and a non-scaled ANN was conducted to evaluate the estimation performance and scale

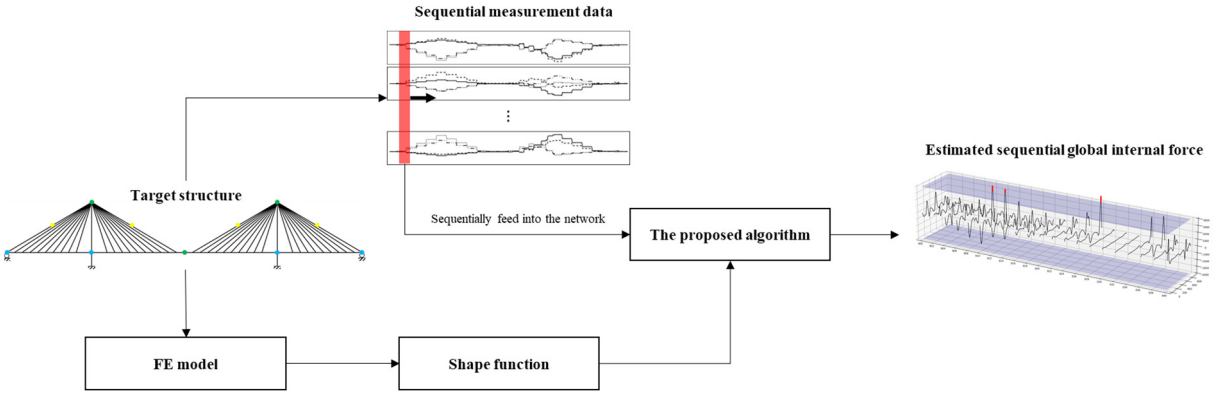

Fig. 16 SHM strategy using the proposed algorithm for static and quasi-static responses

factor effect. The following conclusions can be drawn:

- Displacement, slope, and strain data can be utilized in combination for global response estimation, and additional use of slope and strain data improve the estimation accuracy.
- The scale factor should be considered in the input data and loss for each response to prevent estimation errors due to the scale difference between responses.
- The proposed method shows a more stable and accurate estimation performance for global deformation and internal forces than SRALMR because the former can sufficiently capture local rapid changes in response shape near loading points.

The method developed in this study can be utilized to directly evaluate the integrity of an entire structure based on real-time displacement, slope, and strain data. The estimation of dynamic global responses and experimental validation will be performed in future studies.

Acknowledgments

This work was supported by the National Research Foundation of Korea (NRF) funded by the Korea Government (MIST) [grant No. 2020R1A2C2014450] and by the Basic Science Research Program through the National Research Foundation of Korea (NRF) funded by the Ministry of Education [grant No. 2022R1I1A1A01053382].

References

Breiman, L. (2001), "Random Forests", *Mach. Learn.*, **45**, 5-32.

Byun, N. and Kang, Y.-J. (2023), "Improved estimation method of global deformation and internal forces for cable-stayed bridge using neural network and limited displacement data", Available at SSRN. http://dx.doi.org/10.2139/ssrn.4329171

Byun, N., Lee, J., Won, J.-Y. and Kang, Y.-J. (2022), "Structural responses estimation of cable-stayed bridge from limited number of multi-response data", *Sensors*, **22**, 3745. https://doi.org/10.3390/s22103745

Castellon, D.F., Fenerci, A. and Øiseth, O. (2021), "A comparative study of wind-induced dynamic response models of long-span bridges using artificial neural networks, support vector regression and buffeting theory", *J. Wind Eng. Indust. Aerodyn.*, **209**. https://doi.org/10.1016/j.jweia.2020.104484

Cho, S., Sim, S., Park, O. and Lee, J. (2014), "Extension of indirect displacement estimation method using acceleration and strain to various types of beam structures", *Smart Struct. Syst., Int. J.*, **14**(4), 699-718. https://doi.org/10.12989/sss.2014.14.4.699

Cho, S., Yun, C.-B. and Sim, S.-H. (2015), "Displacement estimation of bridge structures using data fusion of acceleration and strain measurement incorporating finite element model", *Smart Struct. Syst., Int. J.*, **15**(3), 645-663. https://doi.org/10.12989/sss.2015.15.3.645

Choi, J.H., Lee, K.S. and Kang, Y.J. (2017a), "Quasi-static responses estimation of a cable-stayed bridge from displacement data at a limited number of points", *Int. J. Steel Struct.*, **17**, 789-800. https://doi.org/10.1007/s13296-017-6032-6

Cortes, C. and Vapnik, V. (1995), "Support-vector networks", *Mach. Learn.*, **20**, 273-297. https://doi.org/10.1007/BF00994018

Deng, H., Zhang, H., Wang, J., Zhang, J., Ma, M. and Zhong, X. (2019), "Modal learning displacement–strain transformation", *Rev. Scientif. Instrum.*, **90**, 075113. https://doi.org/10.1063/1.5100905

Duan, D.Y., Wang, Z.C., Sun, X.T. and Xin, Y. (2022), "A data fusion method for bridge displacement reconstruction based on LSTM networks", *Smart Struct. Syst., Int. J.*, **29**(4), 599-616. https://doi.org/10.12989/sss.2022.29.4.599

Foss, G.C. and Haugse, E.D. (1995), "Using modal test results to develop strain to displacement transformation", *Proceedings of the 13th International Modal Analysis Conference*, Nashville, TN, USA.

Gulgec, N.S., Takáč, M. and Pakzad, S.N. (2020), "Structural sensing with deep learning: Strain estimation from acceleration data for fatigue assessment", *Comput.-Aided Civil Infrastr. Eng.*, **35**, 1349-1364. https://doi.org/10.1111/mice.12565

Hou, X., Yang, X. and Huang, Q. (2005), "Using inclinometers to measure bridge deflection", *J. Bridge Eng.*, **10**, 564-569. https://doi.org/10.1061/(ASCE)1084-0702(2005)10:5(564)

Kim, S., Won, D.H. and Kang, Y.J. (2016a), "Ultimate behavior of steel cable-stayed bridges - I. Rational ultimate analysis method", *Int. J. Steel Struct.*, **16**(2), 601-624. https://doi.org/10.1007/s13296-016-6027-8

Kim, S., Won, D.H. and Kang, Y.J. (2016b), "Ultimate behavior of steel cable-stayed bridges - II. Parametric study", *Int. J. Steel Struct.*, **16**(2), 625-636. https://doi.org/10.1007/s13296-016-6028-7

Kliewer, K. and Glisic, B. (2019), "A comparison of strain-based methods for the evaluation of the relative displacement of beam-like structures", *Front. Built Environ.*, **15**, p. 118.

https://doi.org/10.3389/fbuil.2019.00118

Koo, K.Y., Brownjohn, J.M.W., List, D.I. and Cole, R. (2013), "Structural health monitoring of the Tamar suspension bridge", *Struct. Control Health Monitor.*, **20**, 609-625. https://doi.org/10.1002/stc.1481

Lei, X., Siringoringo, D.M., Dong, Y. and Sun, Z. (2023), "Interpretable machine learning methods for clarification of load-displacement effects on cable-stayed bridge", *Measurement*, **220**, p. 113390. https://doi.org/10.1016/j.measurement.2023.113390

Lee, H.S., Hong, Y.H. and Park, H.W. (2010), "Design of an FIR filter for the displacement reconstruction using measured acceleration in low-frequency dominant structures", *Int. J. Numer. Methods Eng.*, **82**, 403-434. https://doi.org/10.1002/nme.2769

Li, L., Zhong, B.-S., Li, W.-Q., Sun, W. and Zhu, X.-J. (2017), "Structural shape reconstruction of fiber Bragg grating flexible plate based on strain modes using finite element method", *J. Intell. Mater. Syst. Struct.*, **29**, 463-478. https://doi.org/10.1177/1045389x17708480

Li, J., He, Z. and Fan, G. (2022), "Structural health monitoring response reconstruction based on UAGAN under structural condition variations with few-shot learning", *Smart Struct. Syst., Int. J.*, **30**(6), 687-701. https://doi.org/10.12989/sss.2023.30.6.687

Moon, H.S., Ok, S., Chun, P.-j. and Lim, Y.M. (2019), "Artificial neural network for vertical displacement prediction of a bridge from strains (Part 1): girder bridge under moving vehicles", *Appl. Sci.*, **9**. https://doi.org/10.3390/app9142881

Oh, B.K., Glisic, B., Kim, Y. and Park, H.S. (2019), "Convolutional neural network-based wind-induced response estimation model for tall buildings", *Comput.-Aided Civil Infrastr. Eng.*, **34**, 843-858. https://doi.org/10.1111/mice.12476

Park, K.-T., Kim, S.-H., Park, H.-S. and Lee, K.-W. (2005), "The determination of bridge displacement using measured acceleration", *Eng. Struct.*, **27**, 371-378. https://doi.org/10.1016/j.engstruct.2004.10.013

Park, J.-W., Sim, S.-H., Jung, H.-J., Spencer Jr, B.F. (2013), "Development of a wireless displacement measurement system using acceleration responses", *Sensors*, **13**, 8377-8392. https://doi.org/10.3390/s130708377

Rapp, S., Kang, L.-H., Han, J.-H., Mueller, U.C. and Baier, H. (2009), "Displacement field estimation for a two-dimensional structure using fiber bragg grating sensors", *Smart Mater. Struct.*, **18**, 025006. https://doi.org/10.1088/0964-1726/18/2/025006

Sarwar, M.Z. and Park, J. (2020), "Bridge displacement estimation using a co-located acceleration and strain", *Sensors*, **20**, 1109. https://dx.doi.org/10.20944/preprints202001.0253.v1

Shin, S., Lee, S.-U., Kim, Y. and Kim, N.-S. (2012), "Estimation of bridge displacement responses using FBG sensors and theoretical mode shapes", *Struct. Eng. Mech., Int. J.*, **42**(2), 229-245. https://doi.org/10.12989/sem.2012.42.2.229

Sun, L., Sun, Z., Dan, D., Zhang, Q. and Huang, H. (2009), "Researches and implementations of structural health monitoring systems for long span bridges in China", *JSCE*, **26**, 13s-27s. https://doi.org/10.2208/jsceseee.26.13s

Wong, K.-Y. (2004), "Instrumentation and health monitoring of cable-supported bridges", *Struct. Control Health Monitor.*, **11**, 91-124. https://doi.org/10.1002/stc.33

Wu, R.-T. and Jahanshahi, M.R. (2019), "Deep convolutional neural network for structural dynamic response estimation and system identification", *J. Eng. Mech.*, **145**, 04018125. https://doi.org/10.1061/(asce)em.1943-7889.0001556

Xue, J. and Ou, G. (2021), "Predicting wind-induced structural response with LSTM in transmission tower-line system", *Smart Struct. Syst., Int. J.*, **28**(3), 391-405. https://doi.org/10.12989/sss.2021.28.3.391

Ye, X.-W., Sun, Z. and Lu, J. (2023), "Prediction and early warning of wind-induced girder and tower vibration in cable-stayed bridges with machine learning-based approach", *Eng. Struct.*, **275**. https://doi.org/10.1016/j.engstruct.2022.115261

Zhang, Q., Fu, X., Sun, Z. and Ren, L. (2022), "A smart multi-rate data fusion method for displacement reconstruction of beam structures", *Sensors*, **22**, 3167. https://doi.org/10.3390/s22093167

BS